Reconfigurable Multifunctional Transmission Metasurface Polarizer Integrated with PIN Diodes Operating at Identical Frequencies

Jianyu Lin, Dongying Li, and Wenxian Yu

Shanghai Key Laboratory for Intelligent Sensing and Recognition
Shanghai Jiao Tong University, Shanghai, 200240, China
jianyu.l.wl@sjtu.edu.cn, dongying.li@sjtu.edu.cn, wxyu@sjtu.edu.cn

***Abstract* –** Herein, a reconfigurable multifunctional transmission metasurface polarizer, structured with double Jerusalem crosses and integrated with four PIN diodes, is presented. The bottom Jerusalem cross is rotated by 35° with respect to the top cross. Both numerical and experimental observations reveal that a linearly polarized (LP) outgoing wave is transmitted at approximately 4.0 GHz when subjected to a left-handed circularly polarized (LCP) or right-handed circularly polarized (RCP) incident wave. The transmission efficiency reaches -2.5 dB when all elements are in the ON state. Furthermore, active control of switchable PIN diodes operating in various statuses unequivocally demonstrates the ability to convert an incident wave polarized in the *x* or *y* direction to a LCP or RCP wave, respectively, within the identical frequency band, spanning from 3.6 GHz to 4.3 GHz. This conversion is achieved with a transmission coefficient of -3.5 dB or -4.2 dB at the peak frequency. The proposed metasurface polarizer presents a potentially dynamic method for simultaneously manipulating various polarization conversions of electromagnetic (EM) waves within a desired frequency band.

***Index Terms* –** Multifunctional metasurface, polarization conversion, reconfigurable metasurface polarizer.

I. INTRODUCTION

Polarization, a significant characteristic of electromagnetic (EM) waves, plays a crucial role in polarization imaging, modern communication systems, and radar technology. Conventionally, manipulating the polarization state relies on uniaxial crystals, suffering from their bulky configuration, complex feed systems, and limited polarization states. In recent years, metasurfaces, artificial composites consisting of subwavelength scatterers, have emerged as promising approaches to exhibit strong EM responses, such as zero refractive index [1], asymmetric transmission [2], and perfect absorption [3], offering novel EM characteristics beyond natural materials. Early research focused on passive metasurface polarizers, utilizing gradual geometry changes or layer rotation [4–7]. However, these fixed functions and polarization conversion states do not align with the requirements of contemporary compact communication systems.

By controlling external excitation, a tunable or reconfigurable metasurface equipped with active elements expands the range of possibilities for dynamically manipulating the polarization responses of EM waves [8–10]. For instance, based on the equivalent dipole polarization theory, Kazemi [11] achieved perfect reflection or refraction in a desired direction with orthogonal polarization. In [12], a circular polarization converter demonstrated the production of a circularly polarized (CP) wave with handedness orthogonal to the incident wave. Notably, the PIN diode, known for its compact size and controllable properties in the microwave range, has been shown to integrate into metasurface structures. In [13], a circular polarizer produced an outgoing wave that exhibited circular polarization with orthogonal handedness at dual frequencies. The conversion from linear-to-circular (LTC) polarization was also successfully achieved in reference [14]. However, a limitation in previous studies was the different operating frequencies for LCP or RCP wave, which restricted their practical utility. In [15], an incident wave with *x* polarization direction was transformed into LCP or RCP wave within a frequency range from 9.70 to 9.93 GHz. We propose a LTC polarizer operating within the same frequency band using a double-layer metasurface [16], providing a limited yet practical set of polarization conversion functions at the desired frequency range.

In this paper, a reconfigurable multifunctional transmission metasurface polarizer (MP) depicted in Fig. 1 is proposed, achieving circular-to-linear (CTL) and LTC polarization conversion by controlling the PIN diode states at an identical frequency band, which has not been previously reported. Utilizing the transmission matrix approach, metasurface unit cell comprised two-layered Jerusalem crosses incorporated with four active components of PIN diodes and three-layered feeding network, leading to LTC and CTL polarization conversion. Subse-

Submitted On: June 1, 2023
Accepted On: March 16, 2024

https://doi.org/10.13052/2024.ACES.J.390307

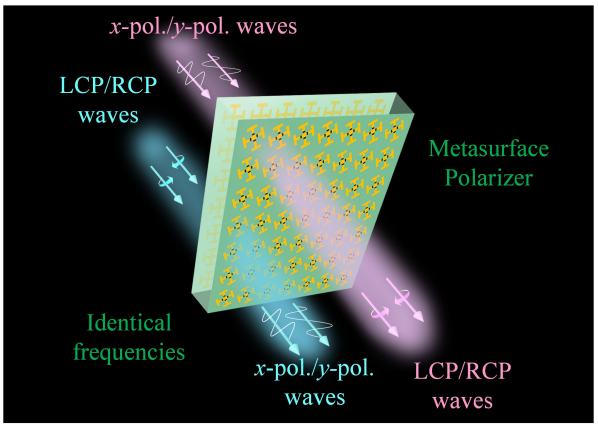

Fig. 1. Schematic of the proposed reconfigurable multifunctional transmission metasurface polarizer.

quently, an 8×8-element reconfigurable multifunctional transmission metasurface polarizer with 256 PIN diodes and 24 inductances was fabricated. The measured performances demonstrate that the emission of an LP wave occurs at approximately 4.0 GHz, with a transmission efficiency of -2.5 dB when all lumped elements are in the ON state, and the structure is illuminated by either a LCP or RCP wave. Furthermore, the ability to convert *x*-polarized and *y*-polarized incident waves to LCP and RCP waves respectively, while maintaining their orthogonal handedness within the desired frequency band of 3.6 GHz to 4.3 GHz, is unambiguously demonstrated with a transmission coefficient of -3.5 dB and -4.2 dB through the active control of the switchable PIN diodes.

II. RECONFIGURABLE UNIT CELL DESIGN

A. Unit cell design

Building upon the structural design introduced in our previous study [16], we present an active and reconfigurable multifunctional transmission metasurface polarizer unit cell. By positioning two Jerusalem crosses and feeding network, we facilitate polarization conversion within the resonance frequency band through the distribution of the surface electric field and cross-coupled magnetic field. The layout of our proposed design is patterned on Rogers RO4350B substrates as shown in Fig. 2 (a). The bottom patch exhibits a twist of 35° relative to the top patch, with other geometric dimensions set as follows: $p = 20$ mm, $g = 1$ mm, $f = 6.8$ mm, $h = 6$ mm, $d = 3.66$ mm, and $b = 4.5$ mm. All Jerusalem crosses are constructed using copper sheets. Additionally, we incorporated various metallic biasing lines (0.4 mm) into the substrate, connecting them to the bottom patch through vertical metallic vias, as illustrated in Figs. 2 (d)-(f).

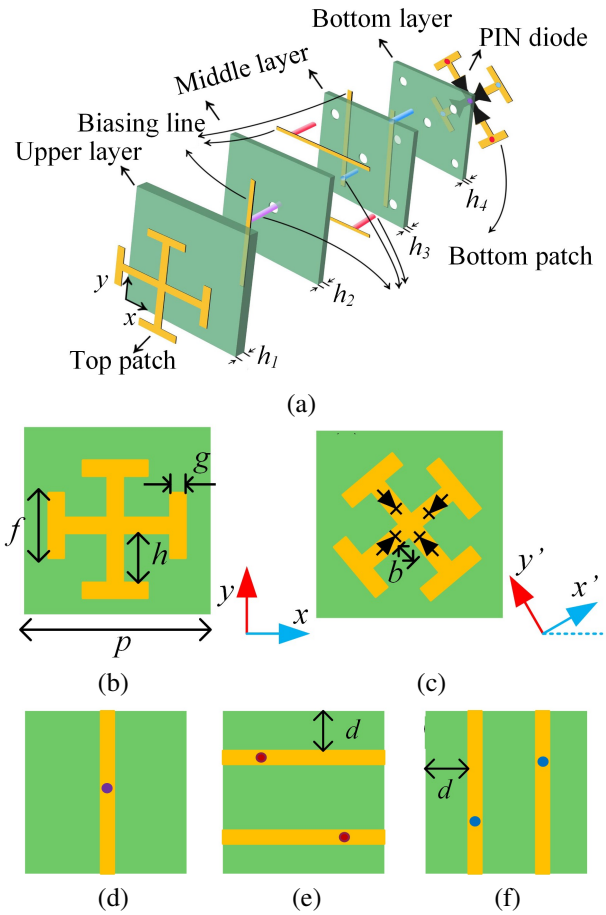

Fig. 2. (a) Layout of the MP unit cell with metallic vias and biasing lines. $h_1 = 0.5$ mm, $h_2 = h_3 = h_4 = 0.3$ mm, (b) top patch on upper layer, (c) bottom patch on bottom layer, and (d)-(f) metallic vias and biasing lines on middle layer.

In our design, the PIN diodes were chosen as MA4AGBLP912 fabricated by MACOM [17] which have ultralow capacitance and series inductance, as well as slight forward resistance and a suitable geometry, thus reducing the mutual coupling and parasitic effect on the structure. The PIN diode can be equivalent to series-parallel RLC circuit with a series inductance of $Ls = 0.5$ nH, reverse resistance of $Rs = 10$ MΩ and a 0.02 pF capacitance in the OFF state. By contrast, a series resistance of $Rs = 4$ Ω is depicted in the equivalent series RL circuit in the ON state. Four lumped elements with equivalent circuit parameters were used to model the PIN diodes by loading them onto a Jerusalem cross over the bottom layer. The four PIN diodes are described as PIN *I*, PIN *II*, PIN *III*, and PIN *IV* arranged counterclockwise. Table 1 shows variable status of those PIN diodes controlled individually.

Table 1: Three status controlled individually

Status I	All ON
Status II	PIN *I* and PIN *III* OFF PIN *II* and PIN *IV* ON
Status III	PIN *I* and PIN *III* ON PIN *II* and PIN *IV* OFF

B. Design principle

To elucidate the EM characteristics of the designed metasurface unit cell, we consider an incident wave that illuminates the upper layer of the unit cell, as depicted in Fig. 3 (a). The top Jerusalem cross patch can be attributed to $C_{4,z}$ symmetry with respect to the z axis, pertaining to the act of rotating an entity by a constant angular measure of 90° around the z axis during each rotation. This action has the ability to align the entity precisely with itself, leading to its unaltered state. All effects associated with circular dichroism can be observed in such systems, as explained by [18]. Consequently, the Jerusalem cross leads to the dual-frequency transmission of LCP and RCP waves in response to an incident wave with circular polarization. Moreover, we observe a pure linearly polarized (LP) wave at frequency f_0 between the dual frequencies, characterized by an ellipticity of zero, demonstrating significant optical activity. As a result, the polarization of $\vec{E}^{t1}$ is linear, not only at the frequency of f_0 for circularly polarized incident waves but also within the arbitrary operational frequency range for LP incidences. We define the transmission parameter T_1 for the top layer as follows:

$$T_1 = \begin{bmatrix} A_1 & B_1 \\ -B_1 & A_1 \end{bmatrix}. \tag{1}$$

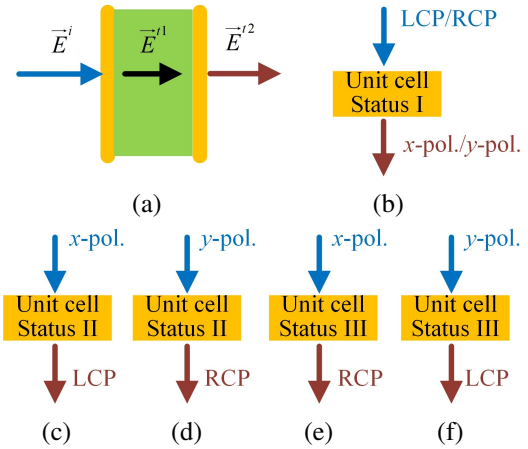

Fig. 3. (a) EM propagation model and (b)-(f) conceptual illustration of incident wave propagation under different status.

In contrast to upper layer, the Jerusalem crosses located on the bottom layer undergoes a counterclockwise rotation about the z-axis with a value of $\varphi = 35°$ and is equipped with four PIN diodes. We then introduce a novel set of coordinates (x', y') by rotating the existing (x, y) system by an angle φ in xOy plane. The transmission parameter T_2 of the bottom layer can be described as follows:

$$\begin{aligned} T_2 &= \begin{bmatrix} t_{x'x'} & t_{x'y'} \\ t_{y'x'} & t_{y'y'} \end{bmatrix} \\ &= \begin{bmatrix} \cos\varphi & -\sin\varphi \\ \sin\varphi & \cos\varphi \end{bmatrix}^{-1} \times T_P \times \begin{bmatrix} \cos\varphi & -\sin\varphi \\ \sin\varphi & \cos\varphi \end{bmatrix}, \end{aligned} \tag{2}$$

where T_P depicts the transmission matrix of identical structure of top layer loaded with four PIN diodes,

$$T_P = \begin{bmatrix} A_P & B_P \\ C_P & D_P \end{bmatrix}, \tag{3}$$

and

$$t_{x'x'} = m^2 A_P + mnB_P + mnC_P + n^2 D_P, \tag{4}$$

$$t_{x'y'} = -mnA_P + m^2 B_P - n^2 C_P + mnD_P, \tag{5}$$

$$t_{y'x'} = -mnA_P - n^2 B_P + m^2 C_P + mnD_P, \tag{6}$$

$$t_{y'y'} = n^2 A_P - mnB_P - mnC_P + m^2 D_P, \tag{7}$$

where $m = cos\varphi$ and $n = sin\varphi$.

Therefore, the total transmission matrix of the proposed unit cell can be described as:

$$T_{total} = T_1 \times T_2 = \begin{bmatrix} A_1 & B_1 \\ -B_1 & A_1 \end{bmatrix} \times \begin{bmatrix} t_{x'x'} & t_{x'y'} \\ t_{y'x'} & t_{y'y'} \end{bmatrix}. \tag{8}$$

When all elements are in the ON state, the structure in second layer also exhibits $C_{4,z}$ symmetry, and T_P and T_2 can be expressed as:

$$T_P = \begin{bmatrix} A_P & B_P \\ -B_P & A_P \end{bmatrix}, \tag{9}$$

$$\begin{aligned} T_2 &= \begin{bmatrix} (m^2+n^2)A_P & (m^2+n^2)B_P \\ -(m^2+n^2)B_P & (m^2+n^2)A_P \end{bmatrix} \\ &= \begin{bmatrix} A_P & B_P \\ -B_P & A_P \end{bmatrix}, \end{aligned} \tag{10}$$

suggesting a pure LP wave and giant optical activity at f_0 for CP incident wave. Furthermore, under Status II or Status III, the capability to transform linear polarization into circular polarization within a specific frequency range is exhibited in Figs. 3 (c)-(f). The intensity of the transmitted waves can then be associated with the intensity of the incident waves via the transmission matrix T_{cl} [13].

$$T_{cl} = \begin{bmatrix} T_{+x} & T_{+y} \\ T_{-x} & T_{-y} \end{bmatrix} = \frac{1}{\sqrt{2}} \begin{bmatrix} t_{xx} + it_{yx} & t_{xy} + it_{yy} \\ t_{xx} - it_{yx} & t_{xy} - it_{yy} \end{bmatrix}, \tag{11}$$

where the RCP component is indicated by $+$, and the LCP component is denoted by $-$. In addition, the transformation coefficients T_{+x}, T_{-x}, T_{+y}, and T_{-y} represent the conversion abilities of the x- and y-components of an LP incident wave impinging on a structure. It is imperative to employ polarization azimuth rotation angle denoted by θ, ellipticity represented by η and polarization extinction ratio denoted by PER to delineate the salient features of the emitted wave comprehensively. The parameters are defined as follows:

$$\theta = \left[\arg\left(E_{+*}\right) - \arg\left(E_{-*}\right)\right]/2, \tag{12}$$

$$\eta = \arctan\frac{|E_{+*}| - |E_{-*}|}{|E_{+*}| + |E_{-*}|}, \tag{13}$$

$$\text{PER} = 20\log_{10}\left(|T_{+*}|/|T_{-*}|\right), \tag{14}$$

where the symbol $*$ indicates the x- or y-polarized component. When $\eta = 0$, the emitted wave is considered an LP wave with rotation angle θ. The PER metric quantifies the disparity between the amplitude of the RCP and LCP outgoing waves.

If incident wave is CP, then Transmission Jones matrix T_{cc} can be adopted to better intuitionally exhibit the transformation efficiencies by considering the circular polarization conversion [18]:

$$T_{cc} = \begin{bmatrix} T_{++} & T_{+-} \\ T_{-+} & T_{--} \end{bmatrix}. \tag{15}$$

C. Simulated results

Based on the previously stated operational principle, a finite element method with frequency-domain solver was utilized in the commercial EM software CST. Figure 4 shows the transmission characteristics of the four lumped elements in the ON state. Under this condition, the overall structure is equivalent to a $C_{4,z}$ asymmetric structure. Therefore, a polarization rotation angle of $\theta = -1.68°$ with $\eta = 0°$ characteristic is presented within the frequency range of 3.0-4.0 GHz, indicating a pure LP emitted wave with a total transmission coefficient of -2.0 dB from a CP incident wave.

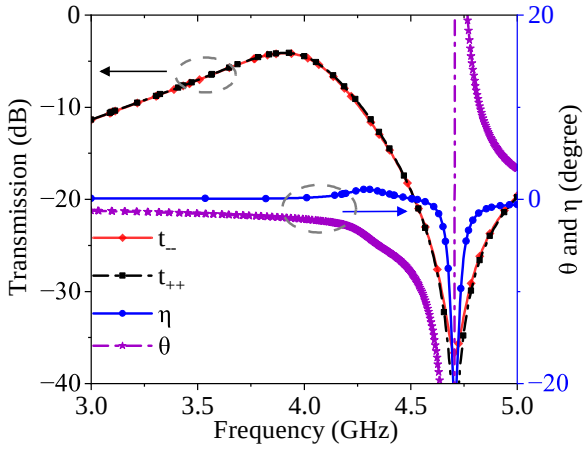

Fig. 4. Transmission coefficients, polarization azimuth rotation angle and ellipticity of MP unit cell for CP incident wave under Status I.

When incidence with x polarization is applied to the structure in Status II, the numerical results illustrated in Fig. 5 (a) indicate that the transmission efficiency of the LCP wave is larger than that of the RCP wave at 3.0-4.5 GHz, whereas the peak intensity of the LCP wave is -2.9 dB at 3.68 GHz, suggesting a prominent LCP emitted wave with $\eta = -5.4°$ and $\theta = -13.4°$. By contrast, the RCP wave is a prominent wave with a transmission efficiency of -3 dB and $\eta = 5.6°, \theta = 12.0°$ at the resonant frequency if the lumped elements are under Status III, as illustrated in Fig. 5 (c). Furthermore, once a y-polarized wave occurs and PIN diodes are arranged with Status II, the RCP wave is the prominent outgoing wave at a frequency of 3.0-4.5 GHz (Fig. 5 (b)), and the transmission efficiency reaches a maximum of -4 dB with polarization azimuth rotation angles of ellipticity $\eta = 8.0°$ and $\theta = -16.2°$ at 4.2 GHz, respectively. Similarly, Fig. 5 (d) shows the LCP polarization conversion from y polarization under the opposing states of the PIN diodes. In conclusion, the most intriguing performance of the MP unit cell should be to actively transmit LP emitted waves from the CP incident wave under Status I and also convert LCP or RCP emitted wave from x- or y-polarized linear wave using switchable PIN diodes under Status II and III.

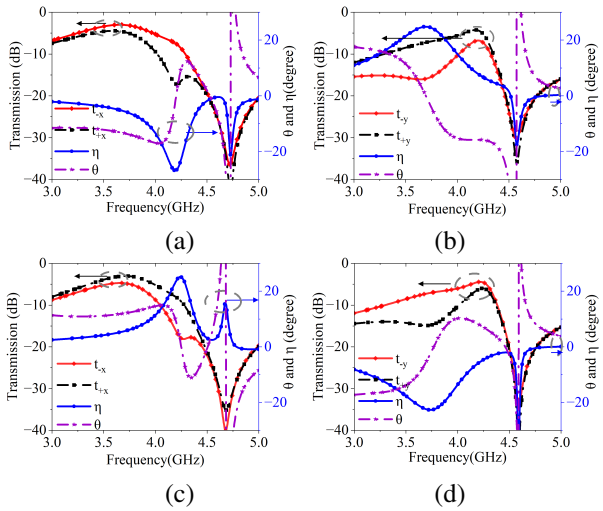

Fig. 5. Simulated switchable properties of MP unit cell. Transmission coefficients, polarization azimuth rotation angle and ellipticity with the PIN diodes under (a) Status II for x-polarized wave, (b) Status II for y-polarized wave, (c) Status III for x-polarized wave, (d) Status III for y-polarized wave.

To clearly explain the physical mechanism of MP unit cell, current distributions at an operation frequency 3.68 GHz for x polarization and 4.2 GHz for y polarization with different PIN diodes states were obtained. As shown in Fig. 6 (a), once the PIN diodes are controlled in Status II and x-polarized wave is incident, the strong surface current (dashed curve) on bottom patch flows along the metallic arm with the PIN diodes in the ON state while the surface current (solid curve) on top patch is concentrated along $-x$ direction at 3.68 GHz, which can be considered as the primary LCP transmitting wave along propagating direction. Similarly, the LCP wave is a prominent transformed wave at 4.2 GHz if the PIN diodes operate in Status III, and a y-polarized wave illuminates the structure in Fig. 6 (e). Moreover, as the current distribution is in the opposite direction in Figs. 6 (c) and (d), the overall result is that the RCP wave is the prominent emitted wave at the operating frequency. Note that the equivalent rotation angles are 125° in Fig. 6 (a) and 145° in Fig. 6 (d), providing different x and y components respectively, and generating different transmittance for the same incident wave with x polarization under Status II and Status III. Obviously, the small difference between x- and y-polarized incidence arises from the effects generated by the asymmetric feeding network. For example, when the incident wave is x-polarized, the surface currents ($\mathbf{J}_2$, $\mathbf{J}_3$, $\mathbf{J}_4$) are mainly located on the biasing lines and can be combined into a black arrow, as shown in Fig. 6 (b). In this case, the synthetic current $\mathbf{J}_0$ can be considered equivalent to an reversed current and counteract the surface currents $\mathbf{J}_4$ flowing along the arm where PIN I and PIN III are OFF. Thus the feeding network has minimal impact on the polarization conversion. For y-polarized incidence, the equivalent current ($\mathbf{J}_2$,$\mathbf{J}_3$) in biasing lines flows along $+y$ direction at 4.2 GHz in Fig. 6 (f), which is contrary to the surface current on top patch, leading to a weakness in the transmittance of y-polarized incident wave under Status III. The manipulation of incident waves with different polarizations within an identical frequency range was realized by dynamically controlling the states of four PIN diodes, distinguishing the proposed design from other polarizers.

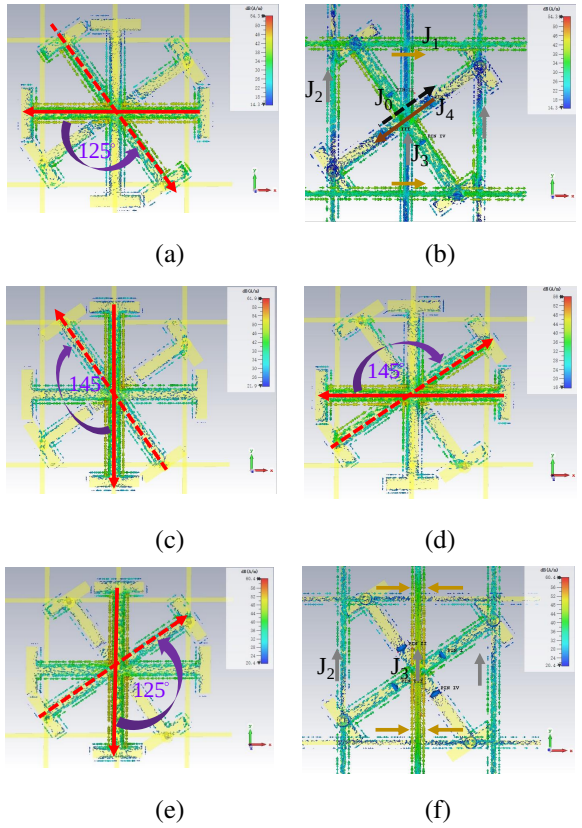

Fig. 6. Surface current distributions of (a) top and bottom patch, (b) and biasing lines, metallic vias under Status II for x-polarized wave at 3.68 GHz, (c) top and bottom patch under Status II for y-polarized wave at 4.2 GHz, (d) top and bottom patch under Status III for x-polarized wave at 3.68 GHz, (e) top and bottom patch, (f) and biasing lines, metallic vias under Status III for y-polarized wave at 4.2 GHz.

III. METASURFACE DESIGN AND PERFORMANCE

In the experiment, the proposed MP prototype comprising 8×8 unit cells was simulated, fabricated, and measured, as shown in Figs. 7 (b) and (c). Simultaneously, 256 PIN diodes connected to a DC bias layer network were demonstrated. Connectivity between the PIN diodes and bias lines was achieved by a large inductance of 16 nH, eliminating RF/DC decoupling and providing the desired isolation in the operation frequency band. The stabilized power supply of Keithley 2231A equipped with three channels in series with 10 Ω resistances provides 1.35 V voltage for each element in the ON state with a forward current of 10 mA. Applying the far-field system, the vector network analyzer of AGILENT N5247A was employed and two identical horn antennas with x and y polarization states were utilized as the transmitter and receiver, as shown in Fig. 7 (a). During measurement, the MP was positioned at the center of the transmitting and receiving antennas with the surrounding microwave absorbing materials to reduce the reflected and diffraction waves. The measurement process comprises distinct components that entail using the same polarization and orthogonal polarization techniques in conjunction with transmitting and receiving antennas operating in three distinct PIN diode statuses, ultimately yielding co-polarized and cross-polarized coefficients. Thereafter, the transmission coefficients of LCP and

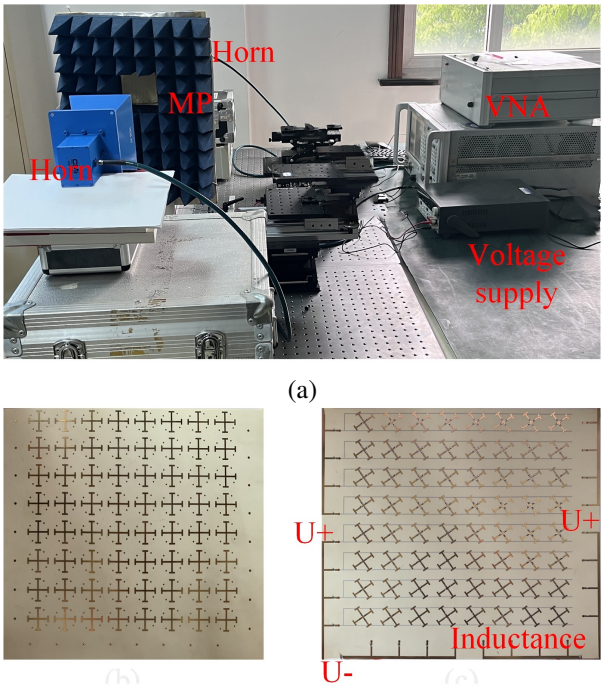

Fig. 7. (a) Measurement system, (b) top view, and (c) and bottom view of the fabricated reconfigurable multifunctional transmission metasurface polarizer.

RCP emitted waves were computed using the transmission matrix.

The measured and simulated scattering parameters of CP incident wave are presented in Fig. 8. By controlling the PIN diodes under Status I, the magnitudes of the LCP and RCP waves are almost identical, demonstrating an LP emitted wave in the vicinity of 4.0 GHz with a total transmission coefficient vale of -2.5 dB and almost zero ellipticity in Fig. 10 (b). Furthermore, the LCP wave is the primary outgoing wave numerically and experimentally within the frequency of 3.6-4.1 GHz for the *x*-polarized incident wave when lumped elements are in Status II. The measured transmission coefficient is above -5 dB within frequency coverage, reaches a maximum of -3.5 dB at 3.74 GHz, and overlaps with the simulated result, as described in Fig. 9 (a). Similarly, the transmittance of RCP wave is observed to be -3.7 dB at 4.0 GHz in Fig. 9 (c) and larger than the LCP wave from 3.6 GHz to 4.1 GHz for *x*-polarized incident wave when PIN diodes are switched to opposite states. For *y*-polarized incidence, the measured transmission coefficients of RCP and LCP components in Status II reach -4.0 dB and -7.0 dB at 4.1 GHz, respectively, as depicted in Fig. 9 (b). Therefore, RCP is the major component within the operational frequency band ranging from 3.95 GHz to 4.3 GHz. Furthermore, the measured transmission coefficient of LCP is -4.2 dB at a peak frequency of 4.0 GHz once the sample is operating in Status III, suggesting that the LCP wave is the outgoing wave. Further, when the frequency increases from 3.86 to 4.24 GHz, the transmission coefficient of the LCP component is above -5 dB, larger than that of the RCP component in Fig. 9 (d). Consequently, the measured results of the fabricated MP operating in various biasing states agreed well with the simulated results. Figure 10 presents the measured ellipticity of the MP. The discrepancy between Status II and Status III for an equivalent normal incidence arises from an incompletely symmetrical structure and feeding network, as well as the loss of PIN diodes. Furthermore, it has been observed that the measured outcome at low frequencies yields unsatisfactory results for both LCP and RCP transmitted waves. This is due to errors resulting from fabrication errors on the surface, as well as a relatively wide beam width in the *y* component at low frequencies generated by horn antennas.

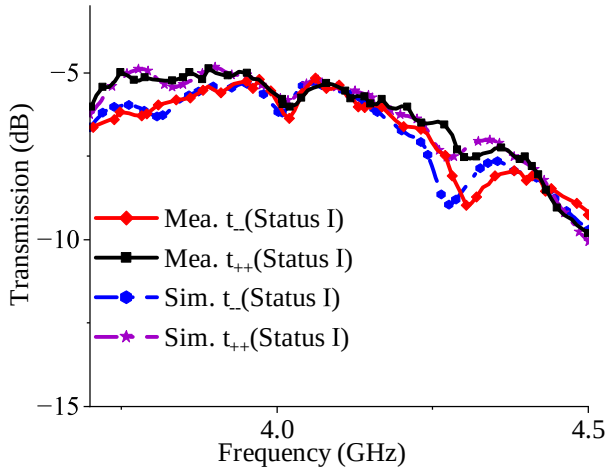

Fig. 8. Measured (solid) and simulated (dashed) properties of the proposed MP under Status I for CP wave.

Table 2 presents a comparison with previously reported CTL and LTC polarization converters. Here, the LTC polarization converters are not reconfigurable and are under *x*- or *y*- polarized incident wave in [19–21]. Both LP and CP waves can be converted into cross-polarization waves; however, they are reflective metasurface polarizers [22]. Most reported metasurface polarizers can only achieve a few types of polarization conversion and operate under dual separate frequency bands. It can be concluded that the proposed design is compact in terms of volume and profile. Meanwhile, the proposed multifunctional transmission metasurface structure can achieve various polarization reconfigurability for both LP and CP incident waves, and it features the identi-

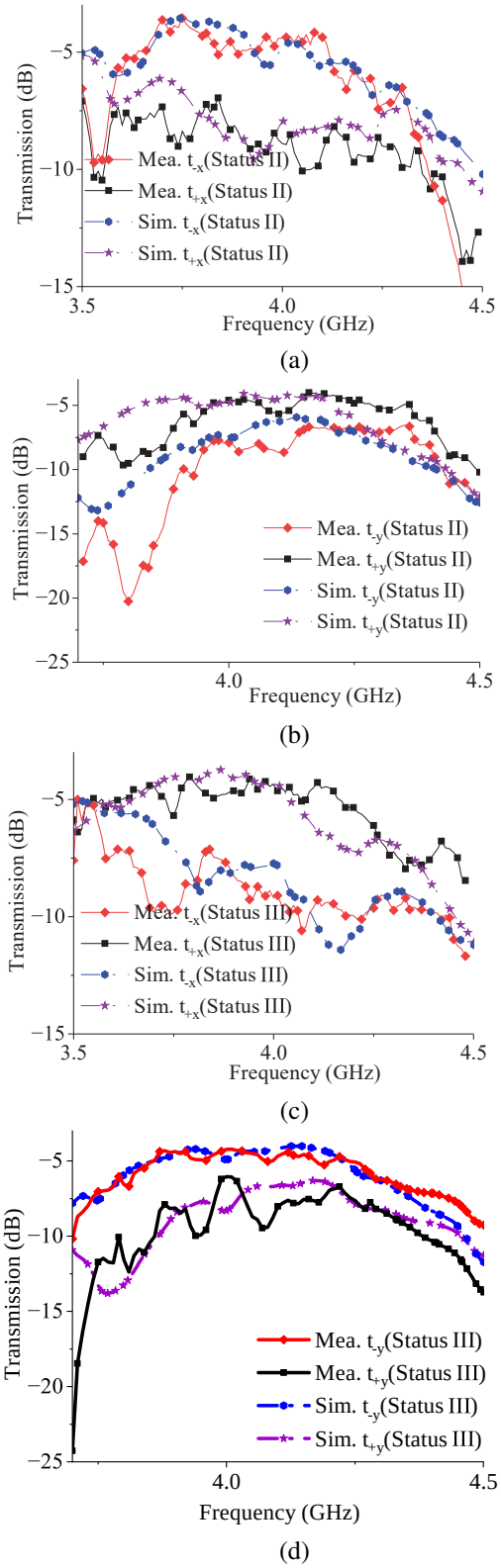

Fig. 9. Measured (solid) and simulated (dashed) properties of the proposed MP under (a) Status II for *x*-polarized wave, (b) Status II for *y*-polarized wave, (c) Status III for *x*-polarized wave and (d) Status III for *y*-polarized wave.

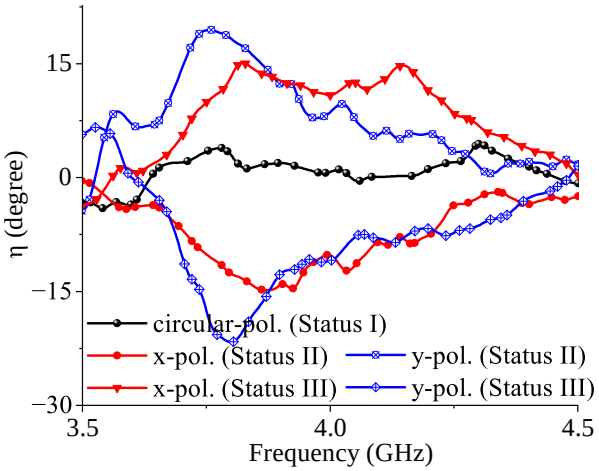

Fig. 10. Measured ellipticity of the MP for circular-, *x*- and *y*- polarized incident wave.

Table 2: Comparisons with previous literatures

Refs.	Thickness (λ)	Reconfigurability	Polarization conversion	Frequency (GHz)	Efficiency (dB)
[19]	0.07	No	*y*-pol. to RCP *y*-pol. to LCP	20 30	-0.1 -0.6
[20]	0.13	No	*x*-pol. to RCP *x*-pol. to LCP	20.1-21.7 29.4-31.4	-1.25 -1
[21]	0.53	No	LP to RCP LP to LCP	19.7-20.2 29.5-30	-0.61 -0.61
[22]	0.10	Yes	LP/CP to orthogonal LP /CP	7.4-12	-1
[23]	0.28	Yes	LP to orthogonal LP	9.7	-0.5
This work	0.02	Yes	CP to LP *x*-pol. to RCP/ LCP *y*-pol. to RCP/ LCP	3.6-4.3	-2.5 -3.5 -4.2

cal operation frequency band. Further investigations are aimed at reducing the loss and improving the transmission efficiency.

IV. CONCLUSION

Herein, a type of dynamically reconfigurable multifunctional transmission metasurface polarizer that can simultaneously manipulate the polarization conversion of linear or circular incident waves within an identical operation frequency range of 3.6-4.3 GHz with switchable PIN diodes was designed, fabricated, and measured. First, we designed a unit cell and illustrated how the structure interacted with the EM waves in terms of current distributions. Subsequently, we revealed that the LP emitted wave is observed in the vicinity of 4.0 GHz through the MP with a total transmission coefficient of -2.5 dB for CP incidence operating in Status I. Moreover, an incident wave in *x*-polarization or *y*-polarization was

simultaneously transformed into left- and right-handed circular polarization in the case of different PIN diodes states within the desired frequency band of 3.6-4.3 GHz, where transmission coefficients of approximately -3.5 and -4.2 dB, respectively, are achieved at peak frequency. This reconfigurable multifunctional transmission metasurface polarizer operating in an identical resonant frequency band provides an innovative and active approach for EM applications.

REFERENCES

[1] V. C. Nguyen, L. Chen, and K. Halterman, "Total transmission and total reflection by zero index metamaterials with defects," *Physical Review Letters*, vol. 105, no. 23, p. 233908, 2010.

[2] C. Huang, J. Zhang, Q. Cheng, and T. Cui, "Multiband tunable asymmetric transmission of linearly polarized electromagnetic waves achieved by active chiral metamaterial," in *2019 Photonics & Electromagnetics Research Symposium-Fall (PIERS-Fall)*, pp. 325-331, IEEE, 2019.

[3] Y. Yao, R. Shankar, M. A. Kats, Y. Song, J. Kong, M. Loncar, and F. Capasso, "Electrically tunable metasurface perfect absorbers for ultrathin mid-infrared optical modulators," *Nano Letters*, vol. 14, no. 11, pp. 6526-6532, 2014.

[4] X. Ni, N. K. Emani, A. V. Kildishev, A. Boltasseva, and V. M. Shalaev, "Broadband light bending with plasmonic nanoantennas," *Science*, vol. 335, no. 6067, p. 427, 2012.

[5] X. Ni, A. V. Kildishev, and V. M. Shalaev, "Metasurface holograms for visible light," *Nature Communications*, vol. 4, no. 1, p. 2807, 2013.

[6] N. Yu and F. Capasso, "Flat optics with designer metasurfaces," *Nature Materials*, vol. 13, no. 2, pp. 139-150, 2014.

[7] G. Ding, K. Chen, G. Qian, J. Zhao, T. Jiang, Y. Feng, and Z. Wang, "Independent energy allocation of dual-Helical multi-beams with spin-selective transmissive metasurface," *Advanced Optical Materials*, vol. 8, no. 16, p. 2000342, 2020.

[8] J. Y. Lau and S. V. Hum, "A planar reconfigurable aperture with lens and reflectarray modes of operation," *IEEE Transactions on Microwave Theory and Techniques*, vol. 58, no. 12, pp. 3547-3555, 2010.

[9] S. Liu and T. J. Cui, "Concepts, working principles, and applications of coding and programmable metamaterials," *Advanced Optical Materials*, vol. 5, no. 22, p. 1700624, 2017.

[10] H. Li, F. Costa, Y. Wang, Q. Cao, and A. Monorchio, "A switchable and tunable multifunctional absorber/reflector with polarization-insensitive features," *International Journal of RF and Microwave Computer-Aided Engineering*, vol. 31, no. 4, p. e22573, 2021.

[11] H. Kazemi, M. Albooyeh, and F. Capolino, "Perfect anomalous reflection and refraction accompanied by an ideal polarization conversion: Potential of a chiral metasurface," in *2019 URSI International Symposium on Electromagnetic Theory (EMTS)*, pp. 1-4, IEEE, 2019.

[12] O. Fernández, A. Gomez, J. Basterrechea, and A. Vegas, "Reciprocal circular polarization handedness conversion using chiral metamaterials," *IEEE Antennas and Wireless Propagation Letters*, vol. 16, pp. 2307-2310, 2017.

[13] S. Yan and G. A. Vandenbosch, "Compact circular polarizer based on chiral twisted double split-ring resonator," *Applied Physics Letters*, vol. 102, no. 10, p. 103503, 2013.

[14] H.-X. Xu, G.-M. Wang, M. Q. Qi, T. Cai, and T. J. Cui, "Compact dual-band circular polarizer using twisted Hilbert-shaped chiral metamaterial," *Optics Express*, vol. 21, no. 21, pp. 24912-24921, 2013.

[15] X. Ma, W. Pan, C. Huang, M. Pu, Y. Wang, B. Zhao, J. Cui, C. Wang, and X. Luo, "An active metamaterial for polarization manipulating," *Advanced Optical Materials*, vol. 2, no. 10, pp. 945-949, 2014.

[16] J. Lin, D. Li, L. Lin, W. Yu, and J. Sheng, "Active transmission-type metasurface for linear-to-Circular polarization conversion at a certain frequency band," in *2023 International Applied Computational Electromagnetics Society Symposium (ACES)*, pp. 1-2, IEEE, 2023.

[17] G. I. Kiani, T. S. Bird, and K. L. Ford, "60 GHz ASK modulator using switchable FSS," in *2010 IEEE Antennas and Propagation Society International Symposium*, pp. 1-4, IEEE, 2010.

[18] J. Zhou, J. Dong, B. Wang, T. Koschny, M. Kafesaki, and C. M. Soukoulis, "Negative refractive index due to chirality," *Physical Review B*, vol. 79, no. 12, p. 121104, 2009.

[19] P. Naseri, S. A. Matos, J. R. Costa, C. A. Fernandes, and N. J. Fonseca, "Dual-band dual-linear-to-circular polarization converter in transmission mode application to K/Ka-band satellite communications," *IEEE Transactions on Antennas and Propagation*, vol. 66, no. 12, pp. 7128-7137, 2018.

[20] M. A. Sofi, K. Saurav, and S. K. Koul, "Frequency-selective surface-based compact single substrate layer dual-band transmission-type linear-to-circular polarization converter," *IEEE Transactions on Microwave Theory and Techniques*, vol. 68, no. 10, pp. 4138-4149, 2020.

[21] J. Lundgren, O. Zetterstrom, F. Mesa, N. J. Fonseca, and O. Quevedo-Teruel, "Fully metallic dual-band linear-to-circular polarizer for K/K a-band,"

IEEE Antennas and Wireless Propagation Letters, vol. 20, no. 11, pp. 2191-2195, 2021.

[22] W. Liu, J. C. Ke, C. Xiao, L. Zhang, Q. Cheng, and T. J. Cui, "Broadband polarization-reconfigurable converter using active metasurfaces," *IEEE Transactions on Antennas and Propagation*, 2023.

[23] Y. Li, Y. Wang, and Q. Cao, "Design of a multifunctional reconfigurable metasurface for polarization and propagation manipulation," *IEEE Access*, vol. 7, pp. 129183-129191, 2019.

Jianyu Lin was born in Zhejiang Province, China, in 1993. He received the B.S. degree in electromagnetic field and microwave technology from Xidian University, Xi'an, China, in 2016 and he is currently working toward the Ph.D. degree at Shanghai Jiao Tong University. His research interests include reconfigurable metamaterial and metasurface, electromagnetic wave regulation and high-gain antennas.

Dongying Li received the Ph.D. degree in electrical engineering from the University of Toronto, Toronto, ON, Canada. He was a Scientist with the Institute of High Performance Computing, Agency for Science Technology and Research, Singapore, from 2011 to 2014. He joined Shanghai Jiao Tong University, Shanghai, China, in 2014, where he is currently an Associate Professor. His research interests include radar target detection algorithms, artificial microwave materials, and antenna design.

Wenxian Yu was born in 1964. He received the Ph.D. degree in communication and electronic system from the National University of Defense Technology (NUDT), Changsha, China, in 1993. From 1996 to 2008, he was a Professor with the College of Electronic Science and Engineering, NUDT. Since 2008, he has been the Executive Dean with the School of Electronic Information and Electrical Engineering, Shanghai Jiao Tong University, Shanghai, China. He is currently the Chief Scientist of information acquisition and processing technology of the National High Technology Research and Development Program of China. His research interests include radar target recognition, remote sensing information processing, and multisensor data fusion.